Mesomorphism and Polar Distortion in 1,4,5,8-Tetrasubstituted Anthraquinones and Anthracenes

Sophie Norvez,* François-Genès Tournilhac, Pierre Bassoul, and Patrick Herson

CNRS, ESA 7071, Chimie Inorganique et Matériaux Moléculaires CIM2, ESPCI, 10 rue Vauquelin, 75231 Paris Cedex 05, France, Université Pierre et Marie Curie, 4 place Jussieu, 75005 Paris, France

Received November 15, 2000. Revised Manuscript Received May 2, 2001

The derivatives of anthraquinone, AQ_n, and anthracene, A_n, substituted with four alkoxy chains $H_{2n+1}C_nO$ ($4 \leq n_{even} \leq 14$) in the 1, 4, 5, and 8 positions were synthesized. All of the molecules, except A_4, yield the smectic A mesophase below the isotropic phase, and with decreasing temperature, ordered smectic phases are observed. For the A_4 molecule, the high-temperature phase is monoclinic with a molecular arrangement of the smectic H type. Single-crystal diffraction of AQ_4 at −50 °C shows a crystalline smectic H′ arrangement and reveals that the molecule is nonplanar. Consequently, the symmetry of the rigid core decreases from D_{2h} to C_{2v}, with a dipole moment along the binary axis. The structures of A_4 and AQ_4 observed in the ordered smectic phases (S_H, $S_{H'}$) afford a picture of well-defined sheets with segregated sublayers. Despite its bowed shape, AQ_4 forms a herringbone arrangement in the aryl sublayer, but with four molecules in the unit cell that are associated in pairs with antiparallel dipole moments. The molecular distortion in 1,4,5,8-tetrasubstituted anthraquinones is proposed as a novel method for introducing a strong dipole moment (about 5 D) perpendicular to the director of a mesogen.

Introduction

Substituted anthraquinones based on 1,4-dihydroxyanthraquinone have occupied a unique place in the field of dyes and pigments because of their brightness and stability.[1,2] More recently, the activity of *N*-alkyl derivatives, such as mitoxanthrone, in cancer chemotherapy has given rise to a new field of interest in anthraquinone chemistry.[3] Anthracene is fluorescent and highly photoreactive. Substituted anthracenes have already been designed for molecular devices such as fluorescent probes for cation detection.[4] Liquid-crystalline phases of anthraquinone or anthracene derivatives offer a potential new route for functionalized molecular materials.

The macroscopic properties of mesomorphic compounds are closely related to the type of organization and symmetry of the mesophase considered. The structure of thermotropic mesophases is highly influenced by the overall shape of the molecules they comprise.[5] Classical mesogens deviate from the isotropic or globular shape with distortion along one direction. The anisotropy of the mesogen is reflected in the parallel alignment of the molecular director in the liquid-crystalline phases. Rodlike (or calamitic) mesogens (Figure 1a) can be likened to prolate ellipsoids and exhibit nematic and smectic phases, whereas disklike mesogens (Figure 1b), with oblate ellipsoidal shapes, give rise to lenticular and columnar arrangements.

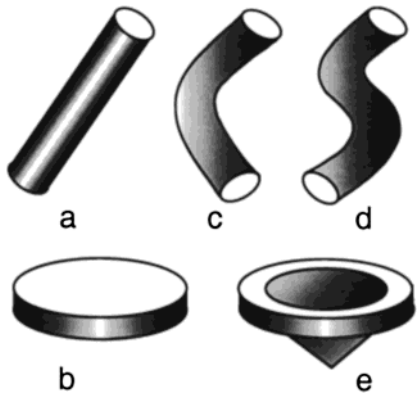

Figure 1. Examples of molecular anisotropy in mesogenic compounds: (a) rodlike, (b) disklike, (c) banana-like, (d) sigmoidal bent-rod, (e) conoidal.

In recent years, spectacular results have been obtained from investigations of new mesogenic architectures that strongly deviate from the simple ellipsoidal models. The magnitude of polarity in chiral smectic C phases was found to be closely dependent on the sigmoidal shape of the molecules[6] (Figure 1d), and new

* Author for correspondence. Mailing address: Department of Chemical Engineering, Stanford University, Stanford, CA 94305-5025. E-mail: sophie@chemeng.stanford.edu.

(1) Zollinger, H. *Color Chemistry*; VCH: Weinheim, Germany, 1991.
(2) Ivashchenko, A. V.; Rumyantsev, V. G. *Mol. Cryst. Liq. Cryst.* **1987**, *150A*, 1−167.
(3) Murdock, K. C.; Child, R. G.; Fabio, P. F.; Angier, R. B.; Wallace, R. E.; Durr, F. E.; Citarella, R. V. *J. Med. Chem.* **1979**, *22*, 1024−1030.
(4) Desvergne, J. P.; Rau, J.; Cherkaoui, O.; Zniber, R.; Bouas-Laurent, H.; Lahrahar, N.; Meyer, U.; Marsau, P. *New J. Chem.* **1996**, *20*, 881−893.
(5) Demus, D *Liq. Cryst.* **1989**, *5*, 75−110.
(6) Walba, D. M.; Slater, S. C.; Thurmes, W. N.; Clark, N. A.; Handschy, M. A.; Supon, F. *J. Am. Chem. Soc.* **1986**, *108*, 5210−5221.

10.1021/cm0009064 CCC: $20.00
Published on Web 07/06/2001

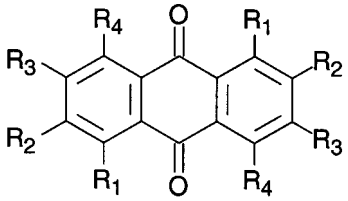

Figure 2. Derivatives of 9,10-anthraquinone in the literature to date. **Ia** $R_1 = H$, $R_2 = R_3 = R_4 = OCOC_nH_{2n+1}$; **Ib** $R_1 = H$, $R_2 = R_3 = R_4 = OC_nH_{2n+1}$; **II** $R_1 = R_2 = R_3 = R_4 = OCOC_nH_{2n+1}$; **IIIa** $R_1 = R_4 = OCOPhC_nH_{2n+1}$, $R_2 = R_3 = H$; **IIIb** $R_1 = R_4 = OCOPhOC_nH_{2n+1}$, $R_2 = R_3 = H$; **IIIc** $R_1 = R_4 = OCOC_nH_{2n+1}$, $R_2 = R_3 = H$.

polar phases were discovered in banana-like smectogens[7] (Figure 1c). Therefore, bent-rod structures have received considerable attention.[8] Polar properties are also expected from conoidal discogens[9] (Figure 1e), and the first examples of this family have been synthesized.[10]

Mesogenic molecules generally consist of a rigid core surrounded by long flexible chains. The number and positions of the chains determine the general shape of the molecule and, hence, the thermotropic liquid-crystalline properties. Rodlike mesogens are typically made of an elongated rigid core, such as biphenyl, substituted with paraffinic end chains, whereas disklike mesogens are generally obtained from planar macrocyclic cores, such as triphenylene,[11] phthalocyanine,[12] or porphyrine,[13] surrounded by six or more flexible chains.

Very few papers have reported investigations of mesomorphic anthraquinone derivatives. The 9,10-anthraquinone core provided the first example of discogenic molecules having lower than 3-fold symmetry. Rufigallol derivatives (1,2,3,5,6,7-hexasubstituted-9,10-anthraquinone I) (Figure 2) show columnar mesophases, in the case of either alkyloyloxy Ia[14,15] or alkyloxy derivatives Ib.[16] Octasubstituted ester derivatives II (Figure 2) also show columnar mesophases.[17] In contrast, anthraquinone derivatives substituted with four lateral side chains in the 1, 4, 5, and 8 positions (IIIa–c, Figure 2) do not show columnar mesophases; the compounds with 4-alkylbenzoate or 4-alkoxybenzoate side chains, IIIa and IIIb, show a smectic mesophase of undefinite nature called "smectic X", and aliphatic ester derivatives IIIc are not mesomorphic at all.[18] This has been attributed to the so-called lath-shape of the molecules. The 1,4,5,8-tetrasubstituted anthraquinone core, which exhibits a shape between disklike and rodlike, does not favor a priori columnar or calamitic arrangements; the disordered smectic A phase has never been observed in this series.

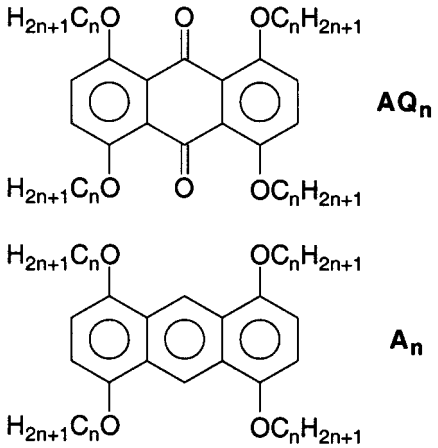

Figure 3. Derivatives of anthraquinone AQ_n and anthracene A_n synthesized.

However, we recently found that 1,4,5,8-tetrakis(1-dodecyloxy)-9,10-anthraquinone, AQ_{12}, and 1,4,5,8-tetrakis(1-dodecyloxy)-anthracene, A_{12}, (Figure 3) present the smectic A phase.[19] At that time, the arrangements of the hard cores and flexible chains within the smectic layers still needed to be understood. In this paper we report the synthesis and structural study of a series of 1,4,5,8-tetraalkyloxy-9,10-anthraquinones, AQ_n, with the chain length n (Figure 3) ranging from butyl to tetradecyl. We investigated the relationship between the molecular shape of these mesogens and the resulting structure of their mesophases. The different types of molecular packing in the smectic phases were analyzed.

The liquid-crystalline properties of the corresponding 1,4,5,8-tetraalkyloxyanthracene derivatives, A_n, are also described. Smectic derivatives based on this rigid aromatic moiety have not been described in the literature to date. Mesomorphic properties of the A_n series are compared to those of the anthraquinone counterparts, focusing on the respective shapes of these apparently similar rigid cores.

Experimental Section

General. NMR spectra were recorded in $CDCl_3$ using a Bruker 300 spectrometer. IR spectra were obtained using a Perkin-Elmer 1600 FTIR spectrometer, and UV spectra using a Uvikon 860 spectrophotometer. Mass spectra were recorded with a GCMS setup using a Hewlett-Packard 5971 detector. Elemental analyses were made in Institut Charles Sadron, Strasbourg, France.

1,4,5,8-Tetrakis(tetradecyloxy)-9,10-anthraquinone (AQ_{14}). A mixture of 1,4,5,8-tetrahydroxyanthraquinone **2** (2 g, 7.35 mmol), Cs_2CO_3 (12 g, 36.8 mmol) and tetradecyl bromide (11 mL, 37 mmol) in DMF (6 mL) was heated at 100 °C for 20 h. After being cooled to room temperature (RT), the mixture was diluted with CH_2Cl_2 and roughly filtered over silica gel prior

(7) Niori, T.; Sekine, J.; Watanabe, J.; Furukawa, T.; Takezoe, H. *J. Mater. Chem.* **1996**, *6*, 1231–1233.
(8) Kishikawa, K.; Harris, M. C.; Swager, T. M. *Chem. Mater.* **1999**, *11*, 867–871.
(9) (a) Petrov, A. G.; Derzhanski, A. *Mol. Cryst. Liq. Cryst.* **1987**, *151*, 303–333. (b) Derzhanski, A.; Petrov, A. G. *Mol. Cryst. Liq. Cryst.* **1982**, *89*, 339–358.
(10) (a) Malthête, J.; Collet, A. *J. Am. Chem. Soc.* **1987**, *109*, 7544–7545. (b) Zimmermann, H.; Poupko, R.; Luz, Z.; Billard, J. *Z. Naturforsch.* **1985**, *40A*, 149–160. (c) Piechocki, C.; Boulou, J. C.; Simon, J. *Mol. Cryst. Liq. Cryst.* **1987**, *149*, 115–120.
(11) Billard, J.; Dubois, J. C.; Nguyen, H. T.; Zann, A. *Nouv. J. Chim.* **1978**, *2*, 535–540.
(12) Piechocki, C.; Simon, J.; Skoulios, A.; Guillon, D.; Weber, P. *J. Am. Chem. Soc.* **1982**, *104*, 5245–5247.
(13) Goodby, J. W.; Robinson, P. S.; Boon-Keng, T.; Cladis, P. E. *Mol. Cryst. Liq. Cryst.* **1980**, *56*, 303–309.
(14) (a) Billard, J.; Dubois, J. C.; Vaucher, C.; Levelut, A. M. *Mol. Cryst. Liq. Cryst.* **1981**, *66*, 115–122. (b) Queguiner, A.; Zann, A.; Dubois, J. C.; Billard, J. *Proceedings of the International Conference on Liquid Crystals*; Chandrasekar, S., Ed.; Heyden and Son: London, 1980; pp 35–40.
(15) Carfagna, C.; Roviello, A.; Sirigu, A. *Mol. Cryst. Liq. Cryst.* **1985**, *122*, 151–160.
(16) Carfagna, C.; Ianelli, P.; Roviello, A.; Sirigu, A. *Liq. Cryst.* **1987**, *2*, 611–616.
(17) Billard, J.; Luz, Z.; Poupko, R.; Zimmermann, H. *Liq. Cryst.* **1994**, *16*, 333–342.
(18) Malthête, J. *C. R. Acad. Sci. Paris* **1983**, *296 II*, 435–437.
(19) Norvez, S. *J. Org. Chem.* **1993**, 2414–2418.

to chromatography in CH_2Cl_2/ether (98:2) or CH_2Cl_2/AcOEt (98:2) mixtures. The desired tetrasubstituted anthraquinone (yellow spot) was crystallized from acetone (52% yield, golden yellow to red crystals). Anal. Calcd for $C_{70}H_{120}O_6$ (MW 1057.72): C, 79.49; H, 11.44. Found: C, 79.17; H, 11.42. IR (KBr, cm^{-1}): 2915, 2849 (CH_3, CH_2), 1683 (C═O), 1577, 1470, 1407, 1280, 1202, 1080, 969, 812, 719 (w). UV (CH_2Cl_2) λ_{max} (nm): 413 ($\epsilon = 8500$). ^1H NMR ($CDCl_3$) δ (ppm): 7.09 (s, 4H, ar), 4.02 (t, $J = 6.6$ Hz, 8H, OCH_2), 1.83 (m, CH_2), 1.50 (m, CH_2), 1.26 (m, CH_2), 0.88 (t, $J = 6.7$ Hz, 12H, CH_3). ^{13}C NMR δ (ppm): 183.0 (q, C═O), 151.1 (q, C−O), 126.2 (q, C ar), 120.1 (t, C−H ar), 70.6 (s, OCH_2), 31.8 (s, CH_2), 29.58−29.20 (CH_2), 25.8 (s, CH_2), 22.5 (s, CH_2), 14.0 (s, CH_3).

1,4,5,8-Tetrakis(dodecyloxy)-9,10-anthraquinone (AQ_{12}) was obtained similarly (81% yield). Anal. Calcd for $C_{62}H_{104}O_6$ (MW 945.5): C, 78.76; H, 11.08. Found: C, 78.08; H, 10.95.

1,4,5,8-Tetrakis(decyloxy)-9,10-anthraquinone (AQ_{10}) was obtained similarly (31% yield). Anal. Calcd for $C_{54}H_{88}O_6$ (MW 833.29): C, 77.83; H, 10.73. Found: C, 78.25; H, 10.67.

1,4,5,8-Tetrakis(octyloxy)-9,10-anthraquinone (AQ_8) was recrystallized from an acetone/methanol 1:1 mixture (74% yield). Anal. Calcd for $C_{46}H_{72}O_6$ (MW 721.07): C, 76.62; H, 10.06. Found: C, 76.52; H, 10.04.

1,4,5,8-Tetrakis(hexyloxy)-9,10-anthraquinone (AQ_6) was obtained similarly (42% yield). Anal. Calcd for $C_{38}H_{56}O_6$ (MW 608.86): C, 74.96; H, 9.27. Found: C, 74.77; H, 9.26.

1,4,5,8-Tetrakis(butyloxy)-9,10-anthraquinone (AQ_4) was recrystallized from ether (67% yield) or from a methanol/water mixture (92:8). MS: *m/z* 496, 439 ($-C_4H_9$), 382 ($-2C_4H_9$), 327 ($-3C_4H_9$), 272 ($-4C_4H_9$). Anal. Calcd for $C_{30}H_{40}O_6$ (MW 496.65): C, 72.55; H, 8.12. Found: C, 72.64; H, 8.16.

1,4,5,8-Tetrakis(butyloxy)-9,10-dihydro-9,10-anthracenediol (DA_4). To a stirring solution of substituted anthraquinone AQ_4 (1 g, 2 mmol) in a mixture of 200 mL MeOH/THF (1:1) was added portionwise ground $NaBH_4$ (3.6 g, 95 mmol) at RT. After 3 h, the discolored solution was poured into an ice/water mixture. The precipitate (white to yellow powder) was filtered off, dried under vacuum (P_2O_5) (theoretical yield). IR (KBr, cm^{-1}): 3550 (OH free), 3400 (OH), 2956−2935−2871 (CH_3, CH_2), 1600, 1497, 1468, 1392, 1272, 1098, 957, 796. ^1H NMR δ (ppm): 6.79, 6.73 (2s, 4, ar), (6.41, d, $J = 6$ Hz; 6.17, d, $J = 3$ Hz, 2H benzylic), 4.0, 3.85 (2m, OCH_2), (3.47, d, $J = 3$ Hz; 2.75, d, $J = 6$ Hz, 2OH), 1.74 (m, CH_2), 1.52 (m, CH_2), 0.9 (m, CH_3). The two OH doublets were removed by D_2O, whereas the H doublets turned into singlets. ^{13}C NMR δ (ppm): Every carbon is of two kinds 151.13−150.73 (2q, C−O), 129.27−126.31 (2q, C), 112.46−111.57 (2t, C−H ar), 68.87−68.67 (2s, OCH_2), 59.54−57.91 (2t, CHOH), 31.44−31.38 (2s, CH_2), 19.28−19.12 (2s, CH_2), 13.80−13.77 (2s, CH_3). *1,4,5,8-Tetrakis(alkyloxy)-9,10-dihydro-9,10-anthracenediols (DA_n)* were synthesized similarly to DA_4.

1,4,5,8-Tetrakis(tetradecyloxy)anthracene (A_{14}). A mixture of the dihydrodiol DA_{14} (1 g, 0.94 mmol) and phenylhydrazine (1 mL, 9.3 mmol) in acetic acid (5 mL) was heated under a nitrogen stream at 90 °C and then at 120 °C for 15 min each time. After being allowed to cool for 2 h, the mixture was filtered and then washed with acetic acid and methanol. After being allowed to dry, the mixture was purified by column chromatography (CH_2Cl_2/cyclohexane 20:80) (yellow spot, fluorescent at 254 nm) and crystallized from heptane (pale yellow crystals) in 42% yield. Anal. Calcd for $C_{70}H_{122}O_4$ (MW 1027.74): C, 81.80; H, 11.96. Found: C, 81.93; H, 12.00. IR (KBr, cm^{-1}): 2928, 2848, 1630, 1468, 1330, 1260, 1191, 1134, 1088, 896, 808, 720 UV (ether) λ_{max} (nm): 323, 346, 368, 391, 413 ($\epsilon_{benzenic} = 10^4$). ^1H NMR δ (ppm): 9.16 (s, 9, 10), 6.62 (s, 4H, ar), 4.15 (t, 8H, $J = 6.4$ Hz, OCH_2), 1.98 (m, CH_2), 1.64 (m, CH_2), 1.26 (m, CH_2), 0.89 (t, $J = 6.7$ Hz, CH_3). ^{13}C NMR (A_8) δ (ppm): 149.06 (q, C−O), 125.35 (q, C ar), 115.17 (t, C−H ar 9,10), 102.28 (t, C−H), 68.27 (s, OCH_2), 31.8 (s, CH_2), 29.41 (s, CH_2), 29.28 (s, CH_2), 26.26 (s, CH_2), 22.6 (s, CH_2), 14.0 (s, CH_3).

1,4,5,8-Tetrakis(dodecyloxy)anthracene (A_{12}) was prepared similarly in 76% yield (AcOEt). Anal. Calcd for $C_{62}H_{106}O_4$ (MW 915.5): C, 81.34; H, 11.67. Found: C, 81.44; H, 11.65.

1,4,5,8-Tetrakis(decyloxy)anthracene (A_{10}) was prepared similarly in 65% yield (acetone). Anal. Calcd for $C_{54}H_{90}O_4$ (MW 803.31): C, 80.74; H, 11.29. Found: C, 80.75; H, 11.29.

1,4,5,8-Tetrakis(octyloxy)anthracene (A_8) was prepared similarly in 60% yield (acetone). Anal. Calcd for $C_{46}H_{74}O_4$ (MW 691.09): C, 79.95; H, 10.79. Found: C, 79.48; H, 10.80.

1,4,5,8-Tetrakis(hexyloxy)anthracene (A_6) was prepared similarly in 75% yield (acetone). Anal. Calcd for $C_{46}H_{74}O_4$ (MW 548.88): C, 78.84; H, 10.10. Found: C, 78.40; H, 10.10.

1,4,5,8-Tetrakis(butyloxy)anthracene (A_4) was prepared similarly in 51% yield (heptane). MS *m/z* 466, 409 ($-C_4H_9$), 353 ($-2C_4H_9$), 297 ($-3C_4H_9$), 240 ($-4C_4H_9$) Anal. Calcd for $C_{30}H_{42}O_4$ (MW 466.66): C, 77.21; H, 9.07. Found: C, 77.42; H, 9.12.

Mesomorphic Behavior Study. Thermal studies were carried out using a Perkin-Elmer DSC7 differential scanning calorimeter (DSC) operating at ±10 °C/min under a nitrogen atmosphere. Microscopic textures were observed using a Leitz Orthoplan polarizing microscope equipped with a Mettler FP52 hot stage.

Structural Characterization. X-ray diffraction powder patterns in the smectic A phase were recorded from capillary samples under vacuum with a Debye−Scherrer chamber, using monochromatic Cu Kα radiation (1.5405 Å). The sample temperature was controlled with an accuracy of ±0.1 °C.

Single-crystal X-ray diffraction experiments were carried out at the Centre de Résolution Structurale de l'Université Paris VI using an Enraf-Nonius CAD4 diffractometer equipped with a liquid-nitrogen cooling stage. The graphite monochromatic Mo Kα radiation ($\lambda = 0.71069$ Å) was used. Data were collected in the $\omega/2\theta$ mode with a θ range of 1−25° and an ω-scan range of $0.8 + 0.345\ tg\theta$. The number of unique reflections collected was 4915 [2388 with $I > 3\sigma(I)$] for AQ_4 at 223K and 2422 [915 with $I > 3\sigma(I)$] for A_4 at room temperature. The structures were resolved by minimizing the function $\sum(w||F_o| - |F_c||^2)$. Structural refinements were done with the PC version of CRYSTALS.[20]

The variable-temperature powder X-ray diffraction technique was used for the polycrystalline A_4. A rotating Lindemann capillary of 1-mm diameter was heated at 114 °C with an air stream, affording a temperature regulation of ±1 °C. Cu Kα radiation was used; the diffracted intensities were measured in the meridian plane using an Inel CPS 120 curved position-sensitive detector with a resolution of 0.14° fwhm. Powder diffraction data were indexed using U-fit software.[21] The accuracy of the fit was better than 0.1° in 2θ for all observed reflections without introduction of any correction factor.

A molecular model of anthraquinone AQ_4 was generated on an IBM RISC System 6000 with the BIOSYM program. Quantum molecular calculations were performed within the framework of the semiempirical AM1 approximation[22,23] using the QCPE MOPAC 6.0 package.[24] Molecular and crystal structure views were generated from crystallographic data and from the output files of MOPAC using MOLDRAW;[25] the compactness calculations were achieved using the FASTVOL module in MOLDRAW.

Results and Discussion

Synthesis. The synthetic method applied to the preparation of 1,4,5,8-tetrakis(alkyloxy)-9,10-anthraquinones AQ_n and 1,4,5,8-tetrakis-alkyloxy-9,10-anthracenes

(20) Watkin, D. J.; Prout, C. K.; Carruthers, R. J.; Betteridge, P. *CRYSTALS*; Chemical Crystallography Laboratory: Oxford, U.K., 1996; Issue 10.

(21) Evain, M. *U-fit V1.3: A Cell Parameter Refinement Program*; IMN: Nantes, France, 1992.

(22) Dewar, M. J. S.; Zoebisch, E. G.; Healy, E. F.; Stewart, J. J. P. *J. Am. Chem. Soc.* **1985**, *107*, 3902−3909.

(23) Stewart, J. J. P. *J. Comput. Chem.* **1989**, *10*, 209 and 221.

(24) Stewart, J. J. P. *MOPAC*, version 6.0; QCPE 455; Quantum Chemistry Program Exchange, Chemistry Department, Indiana University: Bloomington, IN, 1990.

(25) Cense, J. M. *MOLDRAW*; Ecole Nationale Supérieure de Chimie de Paris (ENSCP): Paris, France, 1993.

Scheme 1. Synthesis of anthraquinones AQ_n and anthracenes A_n derivatives

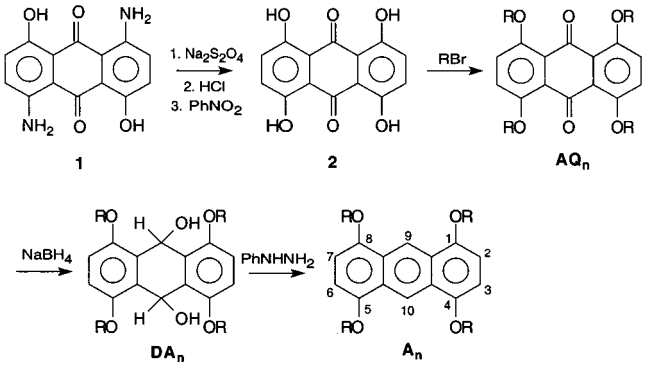

A_n is presented in Scheme 1. 1,4,5,8-Tetrahydroxyanthraquinone (**2**) was obtained from the reaction of sodium dithionite on 1,5-diaminoanthrarufin (**1**), followed by nitrobenzene oxidation.[26] The phenolate of compound (**2**) was reacted with the desired alkyl bromide, giving rise to 1,4,5,8-tetrakis(alkyloxy)anthraquinone, AQ_n. AQ_n was then reduced to 1,4,5,8-tetrakis-(alkyloxy)-9,10-dihydro-9,10-anthracenediol, DA_n, which, in turn, was aromatized by reaction with phenylhydrazine, giving rise to the desired 1,4,5,8-tetrakis(alkyloxy)-anthracene A_n. This method, which was previously described for the dodecyl derivatives,[19] was applied with some changes in purification procedures to synthesize the entire homological series of anthraquinones AQ_n and anthracenes A_n, with $4 \leq n_{even} \leq 14$.

Mesomorphic Behavior. *Anthraquinones AQ_n.* On cooling, the mesophases in all investigated compounds separate from the liquid in the form of *bâtonnets*[27] (Plate 1: Crossed polarizers; full range = 1 μm. Smectic A focal conics texture of AQ_4, 188 °C).

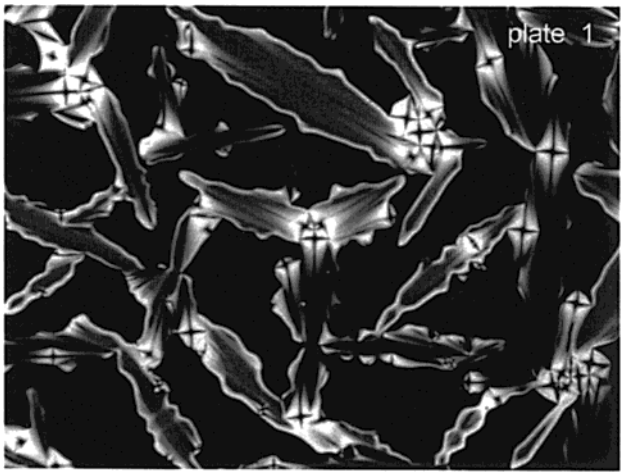

On further cooling, the classical focal conics texture develops. The latter is stable until the appearance of the crystalline phase. The mesophase was identified as smectic A; homeotropic domains were also evident in the same temperature range. The transition temperatures and corresponding enthalpies measured by DSC are listed in Table 1.

The thermal stability of the smectic A (S_A) phase depends on the length of the substituted chains. A maximum range is observed for the AQ_8 and AQ_{10} molecules (Figure 4). From AQ_6 to AQ_{14}, the transition enthalpy between the S_A mesophase and the isotropic liquid (I) does not depend on the chain length ($\Delta H_1 \approx$ 16 J/g). The supercooling value at the clearing point (temperature difference between heating and cooling processes) is almost identical for all of the above compounds ($\Delta T_1 \approx -3.3$ °C at 10 °C/min). This low value is characteristic of the existence of a disordered mesophase below the isotropic liquid. The AQ_4 molecule, with the shortest chain length, exhibits monotropic behavior: its S_A phase is observed only on cooling over a range of 3 °C. The transition enthalpy (−26 J/g) is also significantly larger. In this case, the focal conics texture (and the correlated S_A phase) does not arise if crystalline

Table 1. Phase Behavior of AQ_n Derivatives[a]

AQ_n	C	T_2 (ΔH_2)	S_A	T_1 (ΔH_1)	I	ΔT_1
AQ_4[b]						
heating	•			200.7 (65)	•	
cooling	•	187.3 (−37.5)	•	190.0 (−26.4)	•	
AQ_6	•	139.4 (23.6)	•	168.8 (16.5)	•	−3.5
AQ_8	•	112−115 (34.6)	•	152.5 (16.5)	•	−3.3
AQ_{10}	•	110 (43.6)	•	143 (16.5)	•	−3.3
AQ_{12}	•	110.8 (47.7)	•	131.2 (15.0)	•	−3.2
AQ_{14}	•	114.0 (62)	•	123.5 (15.0)	•	−3.0

[a] The transition temperatures (°C) and enthalpies (J/g) were determined by DSC at 10 °C/min. C, crystalline phase; S_A, smectic A; I, isotropic liquid; ΔH, transition enthalpy; ΔT_1, supercooling at the clearing point. [b] AQ_4 monotropic behavior: the S_A phase is observed only on cooling.

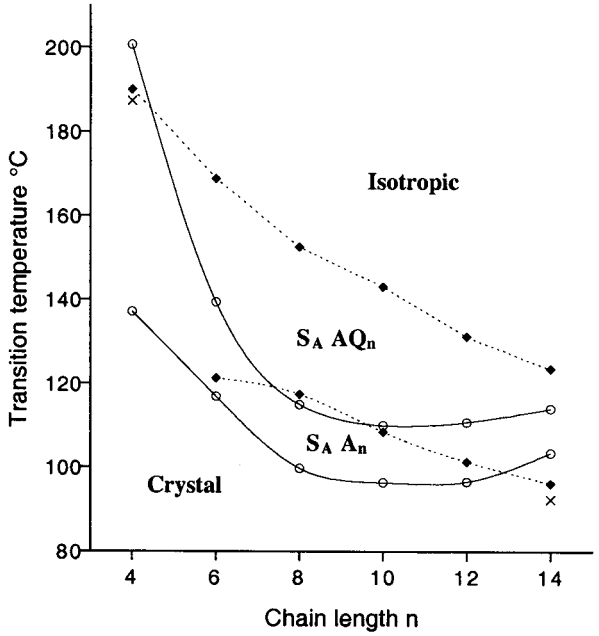

Figure 4. Transition temperatures as a function of the chain length, showing the smectic A domains for anthraquinone AQ_n and anthracene A_n derivatives. ○, C → S_A or C → I (A_4, A_{14}, AQ_4); ◆, S_A ↔ I; ×, S_A (monotropic) → C (AQ_4, A_{14} on cooling). The monotropic behavior of AQ_4 and A_{14} leads to lower temperatures than expected in the case of a regular behavior.

(26) Marshall, P. G. *J. Chem. Soc.* **1937**, 254−255.
(27) Friedel, M. G. *Ann. Phys. France* **1922**, *18*, 273−474.

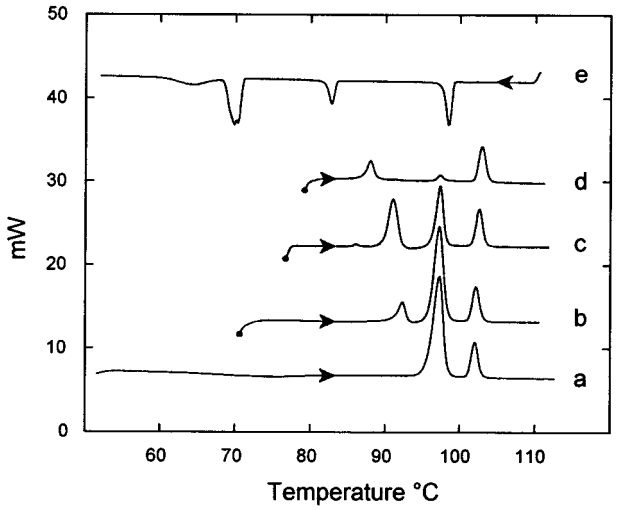

Figure 5. DSC thermograms of anthracene derivative A_{12} depending on different annealing temperatures (●): (a) first heating, (b) after annealing at 70 °C, (c) after annealing at 75 °C, (d) after annealing at 78 °C, (e) first cooling.

nuclei are still present in the liquid. A colorful dendritic mosaic texture then appears (Plate 2: Crossed polarizers; full range = 1 μm. Dendritic mosaic texture of the smectic H′ phase of AQ_4, 197 °C).

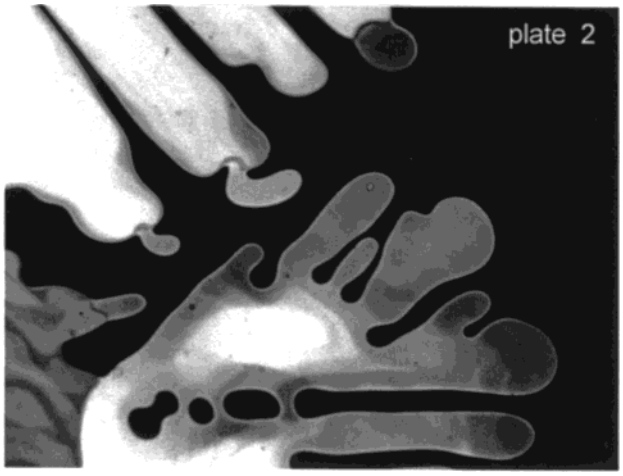

This picture is reminiscent of the growth of biaxial highly ordered smectic phases, separating from the isotropic liquid.[28] It will be shown below that the molecular arrangement of these phases is related to the smectic H′ type.

Anthracenes A_n. All anthracene derivatives A_n, except A_4, present the smectic A phase (Figure 4). However, the thermal behavior of A_n is more complex below the S_A range than it is for the AQ_n crystalline phases. Several ordered phases (generally three) are present. All of them are crystalline and can be more or less favored by annealing at different temperatures. Typical behavior is exemplified by the DSC thermogram of A_{12} (Figure 5).

Transition temperatures and enthalpies for A_n compounds ($4 \leq n \leq 14$) are listed in Table 2. Only the overall enthalpy is given for crystal−crystal transitions, because each single value can change depending on the

(28) Demus, D.; Richter, L. *Textures of Liquid Crystals*; Verlag Chemie: New York, 1987; p. 172.

Table 2. Phase Behavior of A_n Derivatives[a]

A_n	C_{2-4}	T_{2-4} (ΔH_{2-4})	S_A	T_1 (ΔH_1)	I	ΔT_1
A_4	•	97.5				
		112.3				
		137.1			•	−7.9
		(107)				
A_6	•	75.6				
		81.1				
		116.9	•	121.3	•	−2.6
		(85)		(16.5)		
A_8	•	92.8				
		99.8	•	117.4	•	−2.8
		(95)		(17.3)		
A_{10}	•	84.1				
		92				
		96.4	•	108.5	•	−3.7
		(60)		(17.9)		
A_{12}	•	86.6				
		89				
		96.6	•	101.4	•	−3.7
		(60)		(18)		
A_{14}[b]						
heating	•			103.5	•	
				(104)		
cooling	•	74				
		78.1				
		92.4	•	96.2	•	
		(−65)		(−18.1)		

[a] The transition temperatures (°C) and enthalpies (J/g) were determined by DSC at 10 °C/min. S_A, smectic A phase; I, isotropic liquid; C_{2-4}, crystalline phases; T_{2-4} (°C), crystal−crystal transition temperatures; ΔH_{2-4} (J/g), corresponding overall enthalpy; ΔT_1 supercooling at the clearing point. [b] Monotropic behavior.

thermal process. As for AQ_n, the clearing enthalpy, ΔH_1 (about 17 J/g from A_6 to A_{14}), and the supercooling, ΔT_1 (−3 °C at 10 °C/min from A_6 to A_{12}), are almost constant regardless of chain length. Both values are also very close to those recorded for the AQ_n series.

Like AQ_4, anthracene A_4 shows higher values of enthalpy and overcooling at the melting point (twice the value of higher parent compounds). Unlike AQ_4, however, A_4 has no S_A phase. The microscopic texture of A_4 separating from the isotropic liquid is indistinguishable from the dendritic mosaic texture[28] already mentioned for AQ_4 (Plate 3: Crossed polarizers; full range = 1 μm. Dendritic mosaic texture of the smectic H phase of A_4, 134 °C).

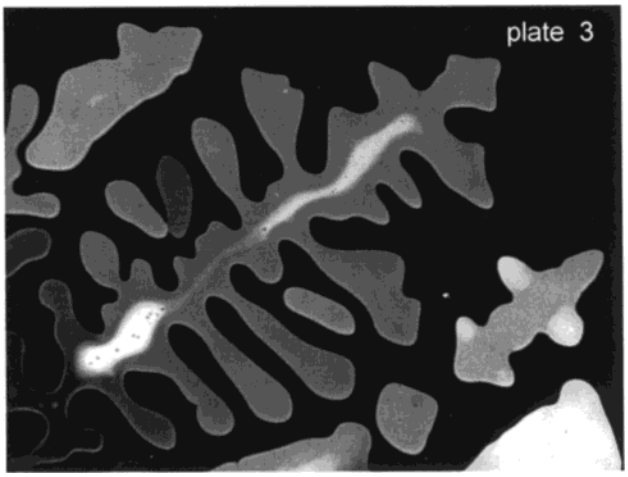

A detailed structural investigation reported in the next section demonstrates that this phase is of the smectic H type.

Table 3. Experimental, d_{exp}, and Calculated, d_n, Interlamellar Distances in the S_A Phases of AQ_n and A_n (Å)

n	C_n[a]	ρ_{flex}	d_n	$d_{exp}AQ_n$	$d_{exp}A_n$
4	2.16	0.90	18.0	16.6[b]	–
6	2.85	0.84	21.5	20.3	20.7
8	3.40	0.80	24.7	24.0	24.1
10	3.85	0.75	27.3	27.3	27.3
12	4.20	0.72	30.1	30.0	31.5
14	4.49	0.69	32.6	32.6	34.4[b]

[a] Extrapolated to short chains from Flory's curve at 140 °C.[29] [b] Monotropic S_A phase for AQ_4 and A_{14}.

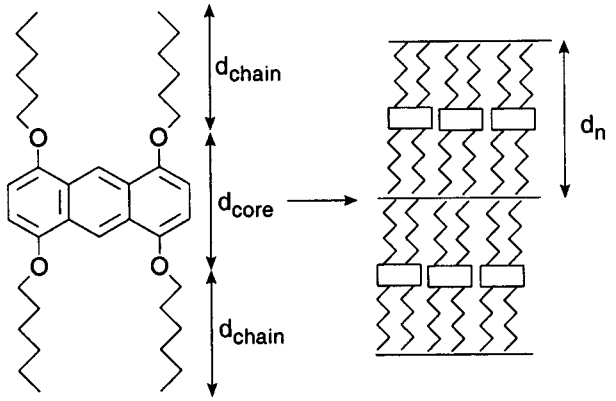

Figure 6. Model of the AQ_n and A_n smectic A mesophases. Only the anthracene core is presented.

At the opposite side of the series, anthracene A_{14} shows monotropic behavior on cooling: the S_A phase is observed within a very short range of decreasing temperature. The corresponding enthalpy is the same (−18 J/g) as for the A_6−A_{12} compounds.

X-ray Diffraction Experiments and Structure Analyses. *Structure of the Smectic A Phase of AQ_n and A_n.* Anthraquinone and anthracene derivatives show, below the clearing point, a disordered lamellar phase. The powder diffraction patterns present a halo with a maximum of intensity at $2\pi/q = 4.5$ Å. At narrow angles, a series of 00l harmonics (from one to three, depending on the chain length) confirm the microscopic identification as smectic A. The interlayer distances d_{exp} are presented in Table 3. In the case of the butyloxy AQ_4 and tetradecyloxy A_{14} derivatives, the smectic A phase is monotropic with a maximum survival time of 10−20 min in the vicinity of the clearing point. X-ray diffraction patterns of these two compounds were recorded by accumulating short exposures. The crystalline nuclei were eliminated by heating the samples above the clearing point between consecutive exposures (AQ_4, 10 times during 6 min at 191 °C with annealing at 205 °C; A_{14}, 8 times during 15 min at 95 °C with annealing at 105 °C).

The layer thickness as a function of chain length is very similar in the two compounds (Table 3). The same structural model can therefore be proposed for the mesophases. In a model in which molecules are standing up in smectic layers (Figure 6), the layer thickness d_n would correspond to the sum of aromatic and aliphatic parts

$$d_n\ (AQ_n \text{ or } A_n) = d_{core} + 2d_{chain} \qquad (1)$$

Molecular lengths can be deduced from crystallographic results and chain length calculations. According to the A_4 crystallographic structure (see below), $d_{core} = 5.53$ Å. The chain length in an extended trans conformation can be calculated according to

$$d_{ext} = l_{OC}\sin(\angle(OCC)/2) + [l_{CC}\sin(\angle(CCC)/2)](n-1) + r_{CH_3} \qquad (2)$$

where l_{OC} and l_{CC} are the lengths of the O−C and C−C bonds, respectively, and r_{CH_3} is the van der Waals radius of the methyl group. Using the tabulated numerical values $l_{OC} \approx 1.43$ Å, l_{CC} =1.52−1.53 Å, $\angle OCC \approx 108°$, $\angle CCC$ = 112−112.5°, and $r_{CH_3} = 2.0$ Å, it follows for alkoxy chains that

$$d_{ext} = 1.89 + 1.265n \qquad (3)$$

In disordered mesophases, flexible paraffinic chains are more or less molten. Consequently, the length to consider is smaller than that of the extended conformation; d_{chain} is better described by a flexible length d_{flex}. The flexible length d_{flex} can be deduced from conformational energies of n-alkanes.[29] As has been pointed out for micelle size calculations,[30] the flexible length of long alkyl chains is related to the fully extended size by the ratio $\rho_{flex} = d_{flex}/d_{ext}$. For polymethylene chains at 140 °C,[29] the calculation has been made using the characteristic ratio C_n defined by

$$C_n = \langle r^2\rangle_0/nl^2 \qquad (4)$$

where $\langle r^2\rangle_0$ is the unperturbed mean-square end-to-end distance for a sequence of n bonds of length l and represents the effect of short-range interactions such as bond angle restrictions and steric hindrances to internal rotation.

For a finite segment of n bonds, the flexibility coefficient can then be expressed as

$$\rho_{flex} = [\langle r^2\rangle_0]^{1/2}/1.265n = l(nC_n)^{1/2}/1.265n \qquad (5)$$

Values of C_n for short chains come from ref 29. The layer thickness in the smectic A phase can thus be calculated as

$$d_n = d_{core} + 2\rho_{flex}d_{ext} \qquad (6)$$

The experimental distances d_{exp} fit the calculated values well for n = 14−6 with less than 5% error (Table 3). The discrepancy is 8% for $n = 4$; in this case, another parameter must be considered. For shorter-chain compounds, the overall molecular size is more sensitive to the ether linkage angle. According to our AM1 calculations, the direction of the butyloxy chains in the AQ_4 extended conformation makes an angle of 27° with respect to the C9−C10 axis. Consequently, the calculated size for AQ_4 with disordered chains is better expressed as

$$d_4 = d_{core} + 2(\cos 27)\rho_{flex}d_{ext} = 16.6 \text{ Å}$$

which fits the experimental data.

(29) Flory, P. J. *Statistical Mechanics of Chain Molecules*; Interscience Publishers: New York, 1969; Chapter 5, p 147.
(30) Tanford, C. *J. Phys. Chem.* **1974**, *78*, 2469−2479.

According to the data of Table 1, the S_A−I transition entropy increases from 23.7 J/(mol K) for AQ_6 to 40.7 J/(mol K) for AQ_{14}. The unexpectedly high value found for AQ_4 [28.7 J/(mol K)] can be related to a restriction of conformational freedom in the S_A phase. For longer chains, because of the higher probability of gauche bonds, the parallelism between chains does not require such a particular conformation.

The model shown in Figure 6, in agreement with the experimental interlayer distances, must also satisfy the close packing requirement within the layer. This model suggests that the central aromatic sublayer is intercalated between two aliphatic sublayers. Such segregated models have already been proposed for rodlike mesogens.[31] One of the parameters permitting the appearance of the mesophase is the matching between core and chain cross-section values.[32] We measured previously in other mesogens a mean core-to-core distance of 5.5 Å between phenyls in the smectic A phase.[33] Assuming a quasi-hexagonal disordered arrangement, we therefore calculated an area of 26 Å^2 per phenyl ring in the smectic A phase, slightly larger than the value recorded in the crystal phase (about 22 Å^2).[34] A comparison between the benzene and anthracene dimensions can be made from their crystal data:[35−37] the occupied volume per molecule of benzene in the orthorhombic form is 126.8 Å^3, and the corresponding value for monoclinic anthracene is 237.1 Å^3, i.e., 1.87 times that for benzene. Because these two cores have the same height, their molecular cross sections differ by the same ratio. Hence, the calculated area of anthracene in the S_A phase can be taken as $26 \times 1.87 = 48.6$ Å^2. Two alkyl chains with a typical cross section of 22−25 Å^2 can be accommodated in this area only if their long axes are perpendicular to the layer plane. The effects of area matching are well reflected by the data of Figure 4. In both series the S_A−I transition temperature decreases with increasing chain length: longer-chain analogues are smectic only at lower temperatures, at which the chains are more linear. The long-chain derivatives A_{12} and A_{14} also have a slightly larger interlayer distance than calculated from the model (Table 4); this means that the chain flexibility cannot exceed a certain limit, determined by the cross section of the anthracene ring.

Structure of the Crystalline Phases of AQ_4 and A_4. Under conditions of existence of the dendritic mosaic texture (just below the clearing point), the powder diffraction patterns of A_4 and AQ_4 showed a series of Bragg reflections in which a simple lamellar ordering was not recognized. At large angles, a large number of reflections is the signature of a crystal rather than a mesophase. Structures of the room-temperature phases of AQ_4 and A_4 were determined for single crystals.

Table 4. Powder X-ray Reflections (°) and the Corresponding Bragg Spacings (Å) of the A_4 Monoclinic Phase[a]

hkl	2θ found	2θ calc	*d* found	*d* calc
001	5.638	5.637	15.66	15.66
200	9.901	9.825	8.93	8.99
201	12.772	12.797	6.93	6.91
402	19.369	19.380	4.58	4.58
400	19.688	19.723	4.51	4.50
210	20.848	20.812	4.26	4.26
112	21.225	21.292	4.18	4.17
211	22.414	22.396	3.96	3.97
310	23.574	23.592	3.77	3.77
404	24.937	24.953	3.57	3.57
412	26.706	26.778	3.34	3.33
312	28.127	28.230	3.17	3.16

[a] Recorded at 114 °C with a position-sensitive detector.The indexing corresponds to a monoclinic cell of parameters $a = 18.97$ Å, $b = 4.84$ Å, $c = 16.51$ Å, $\beta = 108.47°$.

The AQ_4 compound crystallizes into a monoclinic phase stable from −50 °C to its melting point (200.7 °C). In the case of A_4, two crystalline phases were investigated: a triclinic one at room temperature and a monoclinic one just below the melting point. Single crystals of A_4 were obtained, and the triclinic structure was solved. Concerning the A_4 monoclinic phase, a structural model based on variable-temperature powder diffraction experiment is proposed.

1. Monoclinic Phase of AQ_4 (Smectic H′ Type). Anthraquinone AQ_4 was crystallized from a slowly evaporated mixture of methanol and water as large orange crystals (1−2 mm). The structure of AQ_4 cannot be resolved at room temperature with an *R* factor better than $R = 15\%$. The compound crystallizes in the space group $P2_1/a$ with the parameters $a = 14.464$ Å, $b = 12.098$ Å, $c = 17.381$ Å, $\beta = 108.70°$. Measurements achieved at −50 °C allowed the resolution of the structure: the packing at low temperature only differs from the room temperature measurements by slightly shorter values of the cell parameters, namely, $a = 14.284(3)$ Å, $b = 12.054(4)$ Å, $c = 17.311(4)$ Å, $\beta = 109.91(2)°$, $V = 2802$ Å^3. Analysis indicated the space group $P2_1/a$ ($Z = 4$). Least-squares refinement in full matrix converged at a standard crystallographic discrepancy index $R = 8.8\%$ and $R_w = 10.5\%$. Large positional fluctuations were obtained for the vibration ellipsoids of the extremities of the alkyl chains even at low temperature.

The geometry of the tetrasubstituted anthraquinone in the crystalline phase shows a bowed ring system and bent carbonyls (Figure 7). The dihedral angle between benzenic planes is of 24°, and the carbonyl bonds form an angle of 28° with respect to the C9−C10 direction. Such a bent conformation of the anthraquinone core has been explicitly pointed out very rarely.[38,39] Molecular quantum calculations show that the bent conformation indeed minimizes the intramolecular potential. Figure 7a shows the AQ_4 molecular unit deduced from crystallographic data, together with the model calculated using MOPAC (Figure 7b). From examples found in the Cambridge Structural Database, we noticed that two

(31) Skoulios, A.; Guillon, D. *Mol. Cryst. Liq. Cryst.* **1988**, *165*, 317−332.
(32) Guillon, D.; Skoulios, A. *J. Phys. France* **1984**, *45*, 607−621.
(33) Pensec, S.; Tournilhac, F. G.; Bassoul, P. *J. Phys. II France* **1996**, *6*, 1597−1605.
(34) Landolt-Börnstein. *Zahlenwerte und Funktionen aus Naturwissenschaft und Technik*; Springer-Verlag: Berlin, 1971; vol. III/5a; II/5b.
(35) Wyckoff, R. W. G. *Crystal Structures*; Interscience: New York, 1969; Vol. 6−1.
(36) Kitaigorodsky, A. I. *Molecular Crystals and Molecules*; Academic Press: New York, 1973.
(37) Sinclair, V. C.; Robertson, J. M.; Mathieson, A. M. L. *Acta Crystallogr.* **1950**, *3*, 245−251.
(38) Chikashita, H.; Porco, J. A., Jr; Stout, T. J.; Clardy, J.; Schreiber, S. L. *J. Org. Chem.* **1991**, *56*, 1692−1694.
(39) Kim, H.; Schall, O. F.; Fang, J.; Trafton, J. E.; Lu, T.; Atwood, J. L.; Gokel, G. W. *J. Phys. Org. Chem.* **1992**, *5*, 482−495.

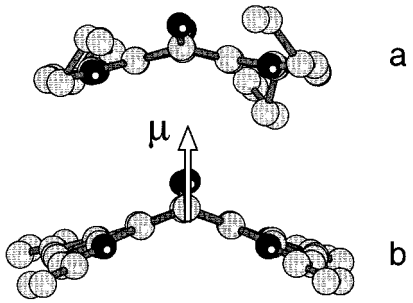

Figure 7. Compared views of anthraquinone AQ_4: (a) deduced from crystallographic data at −50 °C, (b) from MOPAC calculations. The anthraquinone system is not planar and the two carbonyls point up; the resulting dipole moment is shown ($\mu_{calc} = 4.9$ D).

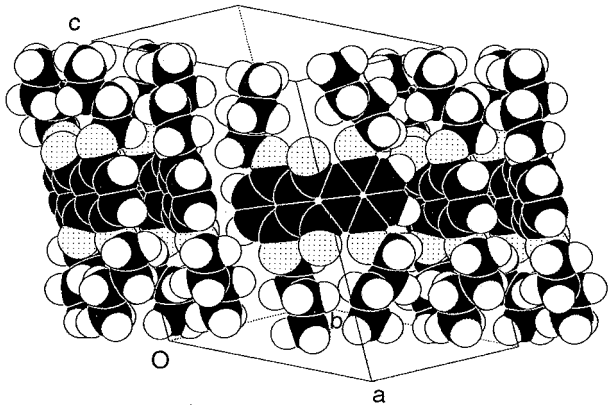

Figure 8. Projection of the monoclinic AQ_4 structure onto the (110) plane. The molecules form a layered arrangement with segregation of alkyl and aryl moieties.

alkoxy[40] or halogen[41] groups in the 1 and 8 positions are sufficient to induce a nonplanar conformation in the crystal phase of substituted anthraquinones. Such an orientation of the carbonyls is likely to be derived from steric interactions with peri substituent groups. As a consequence of nonplanarity, the symmetry of the 1,4,5,8-tetrasubstituted anthraquinone core is not D_{2h} but C_{2v}. These molecules should exhibit a dipole moment along the C_2 axis. The dipole moment calculated using MOPAC is as large as 4.9 D.

The molecular packing of AQ_4 is shown in Figure 8 as a projection onto the $(1\bar{1}0)$ plane. The lamellar arrangement of the S_A phase still exists in the crystalline phase. Considering the crystallographic coordinates it appears that the atomic centers are confined in (001) layers with $0.0063 \leq z \leq 0.9633$. As a consequence, a region with a thickness of 0.7 Å between successive layers is free of any atomic centers. The material can thus be regarded as a stack of well-defined sheets. The interlayer distance is $d = c \sin \beta = 16.28$ Å, slightly shorter than the length of the molecule in its fully extended conformation (18 Å, Table 3). The difference between these values is related to a small tilt of the molecules with respect to the layer normal and to the presence of gauche conformations between the C2 and C3 carbon atoms in the alkyl chains, which are evident in Figure 8. The packing is segregated: aromatic anthraquinone cores locate in a central sublayer, with alkyl chains sublayers on either sides.

The in-plane packing of the aromatic sublayer is presented in Figure 9. Molecules are associated in pairs with antiparallel dipole moments. Molecules in each pair are related to each other by a center of inversion. Projection in the *ab* plane of the aromatic cores shows a herringbone arrangement associated with the *p*2*gg* ^2D space group, with the antiparallel dimer as the repeating unit. The herringbone packing, which is encountered in numerous molecular structures and particularly in smectic phases, corresponds to the close packing of elliptical shapes. An inversion center relating molecules in ^3D corresponds to a 2-fold axis in the ^2D description of the layer. A nonsymmetrical object can pack in *p*2*gg* only in site symmetry 1, which implies four molecules per unit cell. Thus, the bimolecular association of angular anthraquinones is a way of reducing the dipolar electrostatic potential but also a necessary condition for appearance of the herringbone arrangement. The first neighbors of a given dimer are distributed on the nodes of a distorted hexagon. Originating from the center of the hexagon, the *c* axis is tilted toward the apex (inset in Figure 9); hence, the layered arrangement of AQ_4 can be recognized as the crystalline smectic H′ phase.[42]

In the herringbone arrangement of benzene derivatives, the area available per aromatic ring is about 22 Å^2.[34] The expected anthracene cross section in the herringbone arrangement can thus be calculated as previously $22 \times 1.87 = 41$ Å^2. In the *ab* plane of AQ_4, the cross-sectional area per molecule is $ab/4 = 43$ Å^2, close to the previous value, confirming the close packing of angular shapes. In contrast, the area available for each alkyl chain is $ab/8 = 21.5$ Å^2, larger than the typical cross section of crystalline alkanes (18 Å^2).[43] As already mentioned, the alkyl chains in AQ_4 present a gauche conformation between the C2 and C3 carbon atoms and display important positional fluctuations at their extremities. These facts have to be related to a defect of compactness in the alkyl chains stacking. To quantify the empty space existing in the crystal, we calculated its compactness χ as the quantity

$$\chi = \frac{V_k}{abc \sin \beta Z}$$

where $abc \sin \beta$ is the volume of the unit cell and Z is the number of molecules inside. V_k is the Kitaigorodsky volume defined as the envelope of interpenetrating atomic van der Waals spheres.[44] For crystalline anthraquinone, V_k can be calculated from crystallographic data; χ was found to be equal to 0.72. On the other hand, literature data[33,45−48] lead to an average value of $\chi = 0.6$ for smectic materials with crystalline in-plane

(40) Siriwardane, U.; Khanapure, S. P.; Biehl, E. R. *Acta Crystallogr.* **1990**, *C46*, 924−926.
(41) Mikhno, O. A.; Ezhkova, Z. I.; Kolokolov, B. N. *Kristallografiya* **1972**, *17*, 667−670.
(42) Gray, G. W.; Goodby, J. W. *Smectic Liquid Crystals*; Leonard Hill: Glasgow, Scotland, 1984.
(43) Skoulios, *Adv. Colloid Interface Sci.* **1967**, *1*, 79−110.
(44) Reference 36, pp 18−21.
(45) Doucet, J.; Levelut, A. M.; Lambert, M.; Liébert, L.; Strzelecki, L. *J. Phys. Colloq.* **1975**, *36*, 13−19.
(46) Diele, S.; Jaeckel, D.; Demus, D.; Sackmann, H. *Cryst. Res. Technol.* **1982**, *17*, 1591−1598.
(47) Pensec, S.; Tournilhac, F. G.; Bassoul, P.; Durliat, C. *J. Phys. Chem. B* **1998**, *102*, 52−60.
(48) Diele, S.; Jaeckel, D.; Demus, D.; Sackmann, H. *Cryst. Res. Technol.* **1982**, *17*, 1591−1598.

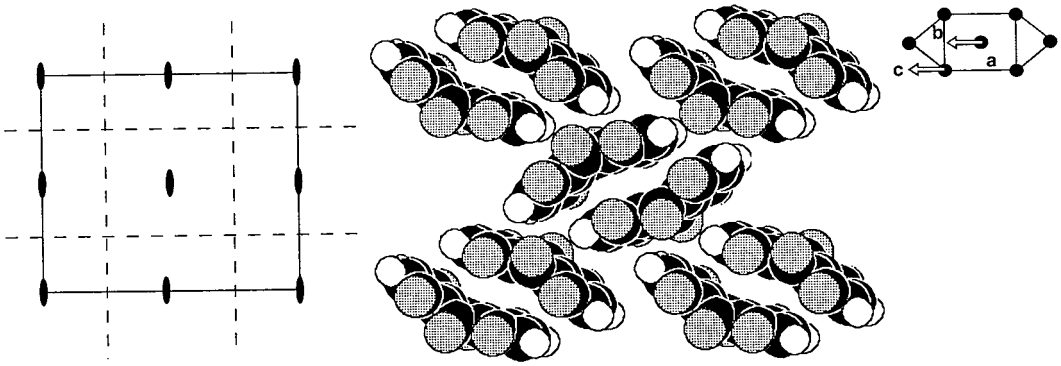

Figure 9. Monoclinic AQ_4 structure viewed as its (001) projection, *ab* plane; only the aromatic cores are shown. The herringbone arrangement of the aromatic sublayer is associated with the ^2D *p*2*gg* space group of the projection. The inset shows the tilt direction of the *c*-axis (arrows).

ordering. The compactness found in the crystalline smectic H′ phase of AQ_4 is intermediate, namely, $\chi = 0.66$. Then the structure of this mesophase appears as a compromise between the alkyl/aryl segregation in smectics and the close packing of the angular cores. The steric matching between aryl and alkyl parts is obtained by a coil conformation of the latter.

2. Triclinic Phase of A_4. Anthracene A_4 was crystallized from heptane as yellow parallepipedic crystals. A single crystal was analyzed by X-ray diffraction at room temperature and found to have the following refined unit cell parameters: $a = 6.250(1)$ Å, $b = 8.178(6)$ Å, $c = 14.141(2)$ Å, $\alpha = 73.69(4)°$, $\beta = 85.01(4)°$, $\gamma = 85.02(6)°$, $V = 689.7$ Å^3. Least-squares refinement in full matrix converged at a standard crystallographic discrepancy index of 4.7% and a weighted residual of 5.9%. Diffraction data are consistent with the $P\bar{1}$ space group ($Z = 1$), with the A_4 molecule located at the center of inversion. A packing model deduced from crystallographic data is presented in Figure 10. The alkoxy chains in the 1 and 5 positions are in all-trans conformation and coplanar with the anthracene core. The direction of these two chains makes an angle of about 27° with respect to the C1−C4 axis. The two other chains (in the 4 and 8 positions) are not planar; the terminal ethyl groups are located symmetrically on either side of the average plane (Figure 10). Two different sublayers, parallel to the (001) plane, are seen in Figure 10. In one type of sublayer, the rigid cores, together with the extended chains, are stacked parallel to each other at a distance of 3.6 Å. The second type of sublayer is composed of the distorted alkyl chains. Hence, a partial segregation between alkyl and aryl groups takes place in the triclinic crystalline phase.

3. Monoclinic Phase of A_4 (Smectic H Type). It can be inferred from textural similarity that the phase occurring just below the isotropic liquid is very similar to the crystalline smectic H′ phase of AQ_4. Because of the lack of single crystals at high temperature, a powder technique was used. Polycrystalline A_4 was analyzed in a rotating Lindemann capillary heated at 114 °C.

The first diffraction peak, later referred to as 001, arises at $2\pi/q = 15.66$ Å. This value is very close to the interlayer distance of AQ_4 in the crystalline $S_{H'}$ phase. This peak was the only detectable harmonic in the 00*l* series (Table 4). Using the structure factors that have been determined for AQ_4 in the crystalline smectic H′ phase and a thermal fluctuation factor σ of 0.5 Å, we found that all 00*l* harmonics are less than 1% of the 001 line, which is the level of the noise in our experiments. The fact that the AQ_4 structure factors are appropriate for explanation of 00*l* intensities in A_4 indicates that both compounds display approximately the same electron density modulation along the direction perpendicular to the layer. The picture of crystalline layers composed of well-defined alkyl and aryl sublayers can therefore be proposed for the high-temperature mesophase of A_4. The powder diffraction data of A_4, together with the proposed indexing, are presented in Table 4. The best fit was obtained with a monoclinic cell of dimensions $a = 18.97$ Å, $b = 4.84$ Å, $c = 16.51$ Å, $\beta = 108.47°$. It is worth noting that *h*0*l* (*h* odd) and 0*k*0 (*k* odd) reflections have not been observed. These extinction rules are consistent with the $P2_1/a$ space group already found in AQ_4. There is no reason for a bimolecular association in the planar A_4 case. Hence, the simple herringbone arrangement with only two molecules in the unit cell in site symmetry $\bar{1}$ can be proposed for this compound. A model of the A_4 in-plane

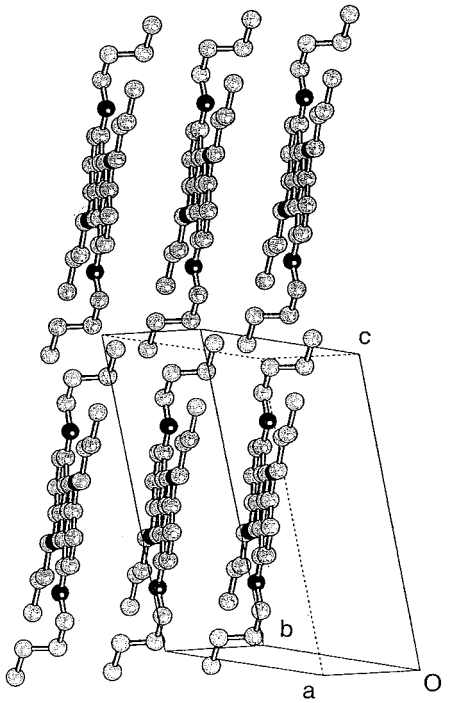

Figure 10. Projection of the A_4 triclinic structure on a plane perpendicular to the anthracene core. The hydrogen atoms are not shown.

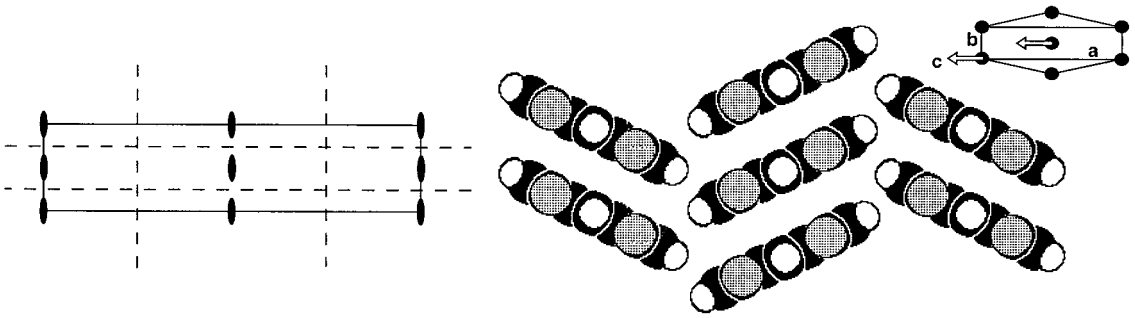

Figure 11. Model of the in-plane arrangement of A_4 in the smectic H form. The symmetry elements of the *p2gg* ^2D space group are shown. The arrows in inset show the tilt direction of the *c* axis.

arrangement is presented in Figure 11. With two molecules in the unit cell, the area allocated to each of them is ab/2 = 46 Å^2. This corresponds to the cross section of anthracene, which is between the values found in the triclinic phase and the smectic A phase. The compactness $\chi = 0.63$ is very close to the value found for AQ_4 in its monoclinic form ($\chi = 0.66$), which also supports the proposed model. As previously, the first neighbors of a given molecule are distributed on the nodes of a distorted hexagon, but in the case of A_4, the tilt direction is oriented toward the edge of the hexagon; this mesophase should therefore be classified as of the smectic H type (inset in Figure 11).[42]

Conclusions

It was demonstrated that anthraquinone and anthracene substituted with four alkyloxy chains in the α positions are liquid-crystalline over a large temperature range. Their smectic A mesophases show similar features at the clearing point: namely, the same enthalpy of transition and overcooling range. However, the domain of existence of the smectic A phase is much larger in the anthraquinone series than in the anthracene series (Figure 4). Moreover, the transition temperatures are much higher for AQ_n than for A_n. This might be related to the bowed conformation of the anthraquinone cores: in the aromatic sublayer, the organization of concave anthraquinones is less likely to be compact than that of planar anthracene, hence increasing the space available for the chains in the aliphatic sublayer. The bending of the anthraquinone core also increases the stability of the crystalline phase, which is reflected by the lack of polymorphism and by higher transition temperatures.

The structures recorded in the ordered smectic phases (crystalline S_H and $S_{H'}$) of A_4 and AQ_4 show well-defined sheets with segregated sublayers. The organization found in the aryl sublayer is of herringbone type, similar to that encountered for rodlike mesogens. The compactness in the monoclinic phases of AQ_4 and A_4 is between those of the ordered smectic and crystalline materials. Thus, the conformational disorder of the alkyl chains seems to be essential for ensuring the cross-section compatibility within the smectic layers. With decreasing temperatures, planar anthracene A_4 undergoes a crystal−crystal phase transition: the rigid core and half of the alkyl chains tend to become coplanar with those of the neighboring molecules. In contrast, in AQ_4, the herringbone arrangement of paired angular molecules is stable down to 223 K.

The model proposed for the disordered smectic A phase, in which molecules stand up in the layers, is clearly supported by the X-ray study of the monoclinic crystalline phases, in which a segregated layered arrangement was evidenced.

The A_n series is the first example of smectic mesogens based on the planar anthracene rigid core. Derivatives of anthracene have already been designed to take advantage of its photophysical properties in different types of molecular materials.[49] In liquid crystals, and particularly in ordered smectics such as smectic H, the orbital overlap might be sufficient to promote a high charge carriers mobility.[50] The smectic phases of the A_n series are therefore potentially photoconductive lamellar fluids.

As a consequence of nonplanarity, 1,4,5,8-tetrasubstituted anthraquinones exhibit a dipole moment (about 5 D) perpendicular to the average molecular plane. The molecular distortion provides a way to introduce a dipole moment parallel to the smectic layers. This is a novel property stemming from the shape of this formally apolar mesogen. The corresponding mesophases are expected to display characteristic properties of polar dielectrics (enhanced permittivity and relaxation phenomena in particular).[51] Electrooptical effects might also be present as a result of coupling between dielectric and optical anisotropies.[52] Experimental investigations of such properties are currently in progress.

Acknowledgments are made to Claude Chassagnard and Colette Jallabert for the NMR measurements, to Robert Cortès and Nicolas Lequeux for their help in X-ray measurements, and to Pr. Jacques Simon for initiating this work.

Supporting Information Available: Tables of crystal data, structure solution and refinement, atomic coordinates, bond lengths and angles, anisotropic thermal parameters, and atomic parameters for hydrogen atoms for anthraquinone AQ_4 and anthracene A_4 (PDF). This material is available free of charge via the Internet at http://pubs.acs.org.

CM0009064

(49) Brotin, T.; Utermöhlen, R.; Fages, F.; Bouas-Laurent, H.; Desvergne, J. P. *J. Chem. Soc., Chem. Commun.* **1991**, 416−418.
(50) Closs, F.; Siemensmeyer, K.; Frey, T.; Funhoff, D. *Liq. Cryst.* **1993**, *14*, 629−634.
(51) Böttcher, C. J. F.; Bordewijk, P. *Theory of the Electric Polarization*; Elsevier: Amsterdam, 1978; Vol. II.
(52) Blinov, L. M. *Electro-Optical and Magneto-Optical Properties of Liquid Crystals*; J. Wiley & Sons: New York, 1983.